Sensors and Materials, Vol. 36, No. 5 (2024) 1835–1848
MYU Tokyo

S & M 3638

Fabrication and Properties of Tungsten-doped Indium Oxide Ultraviolet Photodetector

Artde Donald Kin-Tak Lam,[1] Sheng-Po Chang,[2*]
Chieh-Yu Kuan,[3] and Shoou-Jinn Chang[3]

[1]School of Design & Straits College of Engineering, Fujian University of Technology
No. 3 Xueyuan Road, University Town, Fuzhou City, Fujian Province, China
[2]Department of Microelectronics Engineering,
National Kaohsiung University of Science and Technology, Kaohsiung City 811, Taiwan
[3]Institute of Microelectronics & Department of Electrical Engineering,
National Cheng Kung University, Tainan City 70101, Taiwan

(Received September 8, 2023; accepted April 23, 2024)

Keywords: indium tungsten oxide, photodetectors, cosputtering, annealing, ultraviolet

In this study, we deposit tungsten-doped indium oxide (InWO) thin films as an active layer for ultraviolet (UV) photodetectors (PDs) by radio-frequency (RF) magnetron cosputtering and discuss the optical and electrical properties of the thin film under different process conditions. The introduction of oxygen gas during the thermal annealing of oxide thin films leads to further rearrangement of the lattice and fulfills the oxygen deficiency region. When InWO thin films are thermally annealed in oxygen ambient, its photo–dark current ratio can be greatly improved. Thus, InWO UV PDs with active layers fabricated by cosputtering with sputtering powers of 80 W for the In_2O_3 target and 5 W for the WO_3 target followed by thermal annealing for 1 h in oxygen ambient have the highest performance with an ON/OFF current ratio greater than 10^6, a responsivity of 160 A W^{-1}, and a UV-to-visible rejection ratio of 4.71×10^4. Also, time-dependent switching properties have been demonstrated.

1. Introduction

Ultraviolet (UV) photodetectors (PDs) have many applications, for example, defense warning systems, UV communication, space science, environmental monitoring, industrial production, medicine, and healthcare.[1–6] According to Einstein's explanation of the photoelectric effect based on the photon hypothesis, UV PDs can transform UV radiation signals to photons that can be converted into electrical signals. Therefore, UV PDs have recently attracted much attention. In general, high-performance UV PDs require the merits of high sensitivity, high signal-to-noise ratio, high spectral selectivity, high speed, and high stability, otherwise known as 5S.[7]

It is widely believed that transparent conductive oxides (TCOs) have many excellent properties such as high electron mobility, high optical transparency, good uniformity, good stability, and low-temperature processing.[8] TCOs are regarded as the most promising candidate

*Corresponding author: e-mail: changsp@nkust.edu.tw
https://doi.org/10.18494/SAM4802

ISSN 0914-4935
https://myukk.org/

to replace a-Si:H. Among the many types of TCO, indium oxide (In_2O_3)-based TCO thin films are popular. The conduction bands in In_2O_3-based TCOs originate from the 5s orbital of indium atoms, where the spherically spreading orbital can suppress the perturbing effect. Thus, the In_2O_3-based TCO exhibits excellent electrical conductivity.[9,10] In an InWO lattice system, tungsten serves as a dopant, which not only suppresses oxygen vacancies owing to its high oxygen bond dissociation energy (720 kJ mol^{-1}) but also enhances its stability in the most acidic environment.[11] The tungsten cation, which is W^{6+} in InWO thin films, can supply three extra electrons when substituted for In^{3+}, resulting in an n-type TCO. Thus, InWO thin films have low resistivity and high transparency in the visible region.[12] In addition, they can significantly control the number of oxygen vacancies in InWO thin films owing to their high valence state. Moreover, unlike other In_2O_3-based thin films with low transparency in the near-infrared region (NIR), the high valence state of the tungsten cation improves the transparency of InWO thin films in the NIR.[13] The bandgaps of In_2O_3 and WO_3 are about 3.75 and 3.0 eV, respectively.[14] The bandgap of InWO can be adjusted by changing the tungsten doping ratio. Recent studies have shown that the bandgap of InWO can be tuned from 3.78 to 4.05 eV. Thus, by combining the above characteristics, InWO is a highly promising candidate for UV PD applications.

Numerous types of semiconductor detector structures have been reported, such as the p–n junction, p–i–n photodiode, avalanche, and metal–semiconductor–metal (MSM) structures.[15] Owing to its ease of fabrication and low capacitance, the MSM structure is chosen to fabricate the InWO UV PDs in this study.

2. Experimental Methods

A schematic of the structure of an InWO thin-film UV PD is illustrated in Fig. 1. The fabrication process is described as follows. First, quartz substrates were cleaned using an ultrasonic oscillator in the following sequence: acetone, isopropyl, and deionized water. After cleaning, the samples were dried with nitrogen gas. Second, 200-nm-thick InWO thin films were deposited on quartz substrates by the radio frequency (RF) cosputtering technique with different tungsten doping ratios obtained by adjusting the WO_3 target cosputtering power with the In_2O_3 target cosputtering power set to 80 W at room temperature. To analyze the effect of the tungsten doping ratio on InWO thin-film UV PDs, the modulated WO_3 target cosputtering power was set

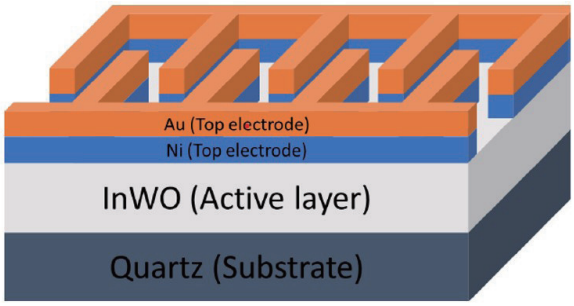

Fig. 1. (Color online) Schematic of the structure of InWO thin-film UV PDs.

at 5 W (4 wt%), 10 W (11 wt%), 20 W (19 wt%), and 30 W (24 wt%). The total gas flow rate was fixed at 50 sccm with an argon gas flow rate of 47 sccm and an oxygen gas flow rate of 3 sccm. Before deposition, the cosputtering chamber pressure was pumped down to less than 5×10^{-6} Torr over 10 h. The chamber pressure was maintained at 5 mTorr during cosputtering, and the holder was rotated 15 times per minute. Also, the angle between the holder and the sputtering gun was 30°, and the distance between the substrate holder and the target gun was 9 cm. Third, Ni/Au (30/70 nm) metal contacts as top electrodes above the InWO thin films were deposited by thermal evaporation with an interdigitated shadow mask, which defines the active region of InWO thin-film UV PDs. Finally, to investigate the effect of the thermal annealing process on InWO thin-film UV PDs, some samples were placed in a furnace in a vacuum or with oxygen ambient for 1 h at 100 ℃.

The electrical and optical properties of InWO UV PDs were measured using a semiconductor parameter analyzer (Agilent Technologies B1500A) at room temperature in a dark chamber. To calculate the responsivity spectra of InWO UV PDs, light illumination was carried out using a 250 W xenon lamp light source, which included a monochromator to provide monochromatic light. In addition, an X-ray diffraction (XRD) analyzer (Bruker AXS D2 PHASER) and an X-ray photoelectron spectroscopy (XPS) system were used to verify the properties of the deposited thin films.

3. Results and Discussion

To analyze the effect of the tungsten doping ratio on InWO thin films, XPS spectra of oxygen 1s orbitals (O1s) are deconvolved into three peaks by Gaussian fitting. The results are shown in Fig. 2. Firstly, the peak O_I at 529.4 eV is attributed to oxygen-lattice bonds, which are related to the oxygen ions combined with the tungsten and indium atoms in the InWO thin films. Secondly, the peak O_{II} at 531.1 eV corresponds to the oxygen vacancy bond. The peak O_{II} is due to oxygen ions that are in an oxygen-deficient region of the a-InWO lattice matrix. Thirdly, the peak O_{III} at 531.6 eV is that of oxygen–hydroxide bonds. Peak O_{III} is associated with the loosely bound oxygen at the InWO thin film surface, which can be regarded as a specific chemisorbed oxygen, such as CO_2, H_2O, or O_2.[16]

Next, the effects of the WO_3 target cosputtering power on the electrical properties of oxygen vacancy are calculated. The oxygen vacancy ratio can be defined as the area under peak O_{II} divided by that under all oxygen 1s orbital peaks, $O_{II}/(O_I + O_{II} + O_{III})$. In general, increasing the oxygen vacancy ratio will increase the number of carriers for TCO thin films and also give rise to some stability issues of devices. The relative oxygen vacancy ratios of O_I, O_{II}, and O_{III} in InWO thin films are summarized in Table 1. The results indicate that the oxygen vacancy ratio decreases with the increase in WO_3 target cosputtering power. This can be explained by the tungsten atom having a higher oxygen bond dissociation energy (720 kJ/mol) than the indium atom (346 kJ/mol),[17] enabling it to bond with the oxygen atom more stably, resulting in the reduction in the number of oxygen vacancies in InWO thin films during sputtering. The oxygen deficiency ratio shows the same trend as the Urbach energy, which agrees with the results of our analyses.

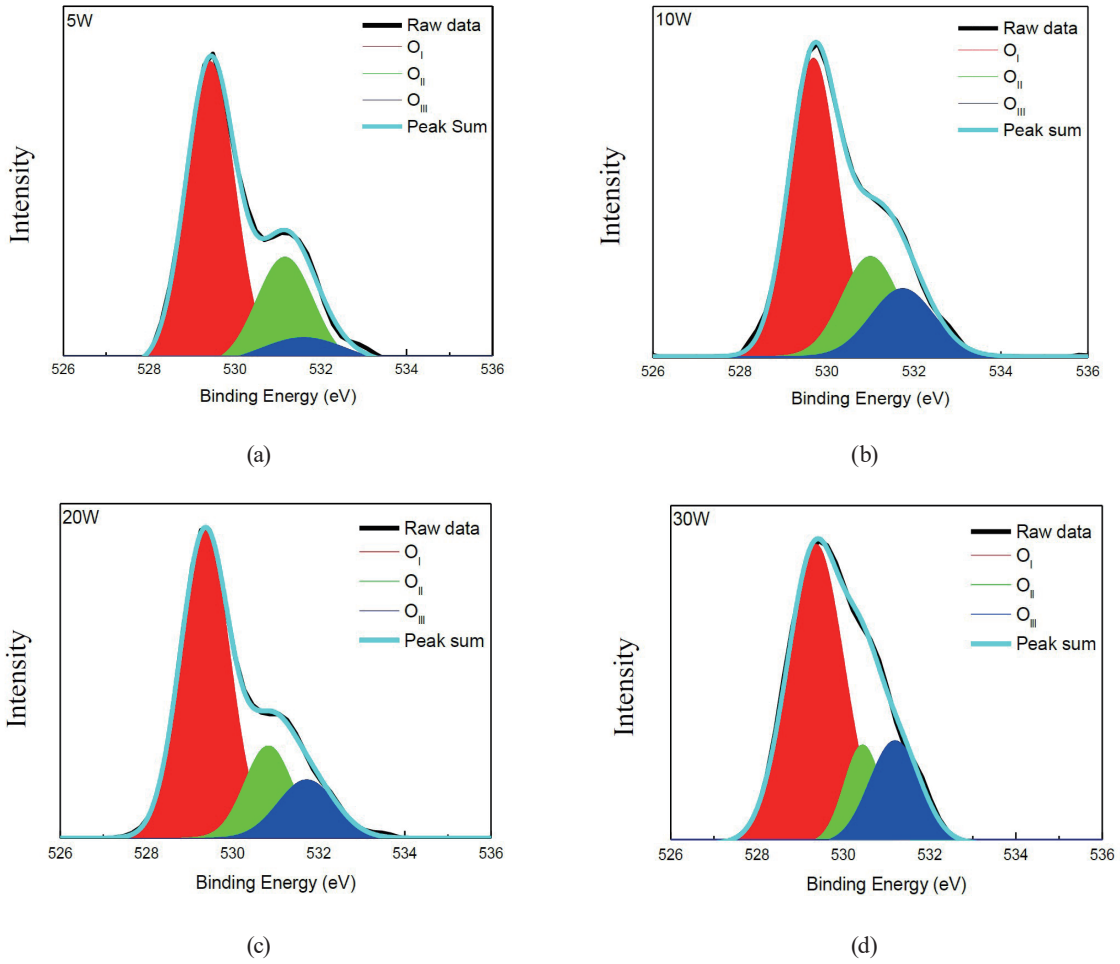

Fig. 2. (Color online) XPS spectra of oxygen 1s orbitals with different WO_3 target cosputtering powers: (a) 5, (b) 10, (c) 20, and (d) 30 W.

Table 1
Relative oxygen vacancy ratios of O_I, O_{II}, and O_{III} in InWO thin-film samples.

Power (W)	O_I ratio	O_{II} ratio	O_{III} ratio
5	64.0	26.2	9.8
10	59.4	23.1	17.5
20	66.2	19.1	14.7
30	65.7	14.1	20.2

Moreover, to verify the elimination of oxygen vacancies by thermal annealing in oxygen ambient, the XPS spectra of oxygen 1s orbitals (O1s) of InWO thin films deposited with different WO_3 target cosputtering powers and treated by thermal annealing in oxygen gas ambient are measured. The relative areas under peaks O_I, O_{II}, and O_{III} are illustrated in Fig. 3 and relative ratios are shown in Table 2. It can be clearly observed that after thermal annealing in oxygen gas ambient, the relative area of O_{II} gradually decreases. This result confirms the suppression of oxygen vacancies by the extra oxygen atoms provided by the oxygen ambient. This agrees with the results of the Urbach energy analysis.

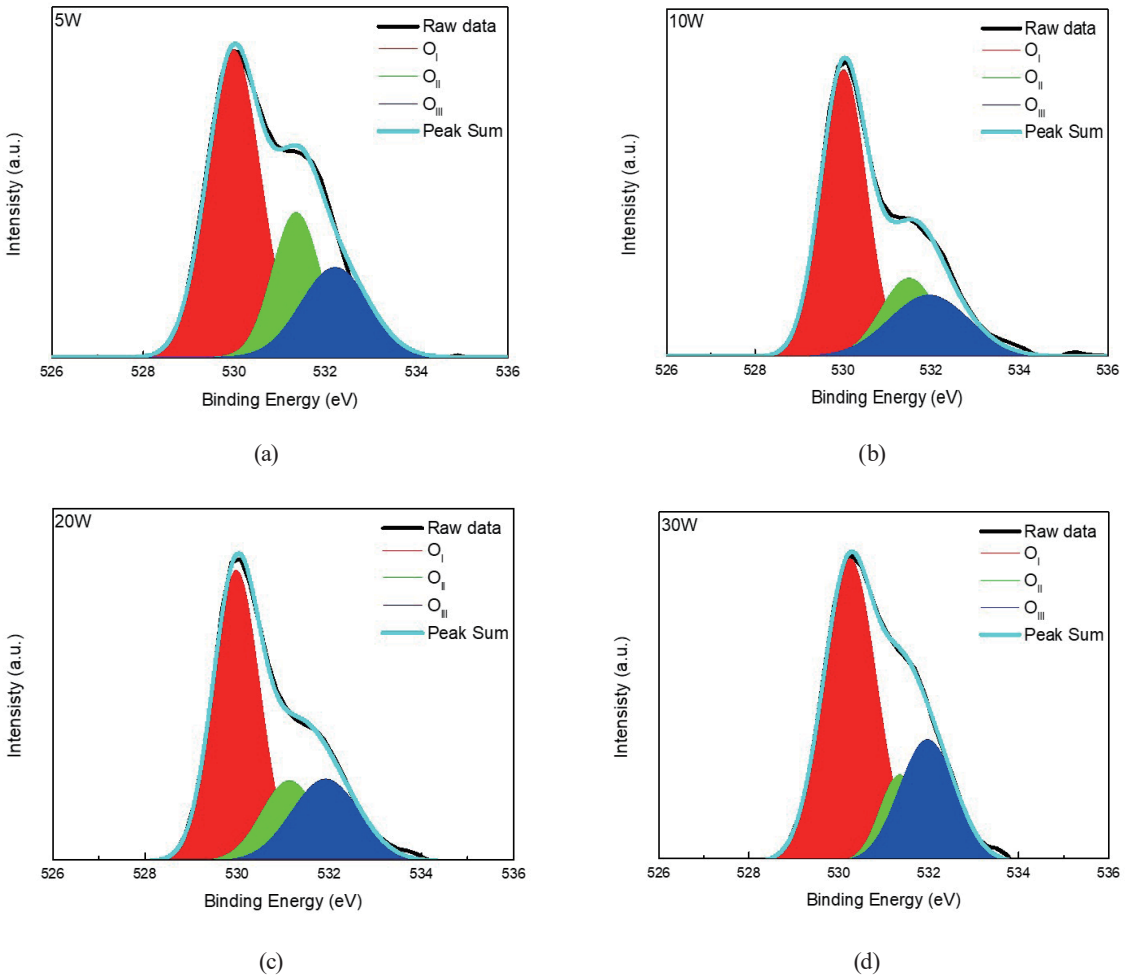

Fig. 3. (Color online) XPS spectra of oxygen 1s orbitals with different WO_3 target cosputtering powers and thermal annealing in oxygen ambient: (a) 5, (b) 10, (c) 20, and (d) 30 W.

Table 2
Relative ratios of O_I, O_{II}, and O_{III} in InWO thin-film samples thermally annealed in oxygen ambient.

Power (W)	O_I ratio (%)	O_{II} ratio (%)	O_{III} ratio (%)
5	55.9	23.3	20.8
10	58.4	19.5	22.1
20	57.6	18.8	23.6
30	61	12.9	26.1

The XRD spectra of InWO thin-film samples with different WO_3 target cosputtering powers are illustrated in Fig. 4. XRD analysis reveals that the lattice structure of InWO thin films is similar to that of indium oxide thin films, that is, a cubic phase of the rhombohedral structure. This result indicates that doping tungsten atoms into indium oxide thin films does not change the lattice structure. Because the atomic radii of indium (0.164 nm) and tungsten (0.144 nm) atoms are close,[18,19] the substitution of tungsten atoms for the indium atoms of indium oxide will not distort the lattice arrangement. According to JCPDS card 74-1410, the diffraction peaks

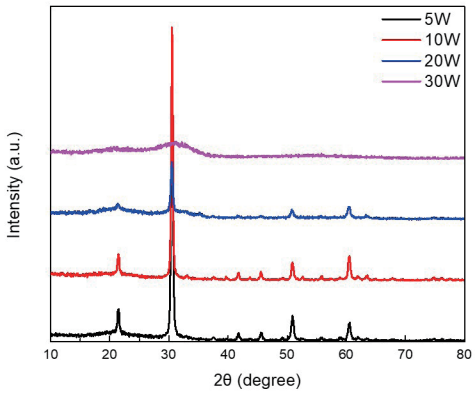

Fig. 4. (Color online) XRD spectra of InWO thin-film samples.

at 23.8, 30.5, 50.3, and 60.6° correlate with (211), (222), (440), and (444), respectively. Thus, the thin films deposited in this work are indeed W-doped indium oxide.

The UV–vis transmittance spectra of InWO thin films thermally annealed in various gas ambients are shown in Fig. 5. The results show that the InWO thin films have good transmittance in the visible light region. The results also show that such thin films have strong absorption in the UV light region, which makes them valuable for sensing UV light. After thermal annealing, the bandgap of the InWO thin films slightly increases, as can be observed from the Tauc plot in Fig. 6. The increasing bandgap can be explained by the decrease in the work function of the InWO thin films after thermal annealing; also, the Fermi level will increase even if the thermal annealing temperature is only 100 °C. The calculated bandgaps of the InWO thin films are summarized in Table 3. According to the results, InWO has an excellent ability to sense UV light owing to its wide bandgap. Because of this characteristic, various InWO thin films were used as the active layer of UV PDs to examine the properties of light sensitivity.

The current–voltage characteristics of unannealed InWO UV PDs in the dark and under illumination are illustrated in Fig. 7. All samples have an ohmic contact between the electrode and the active layer. With an applied bias of −10 V, both the dark current and photocurrent of the sample show the same increasing trend with increasing tungsten doping ratio. The dark/photocurrents for PDs with InWO having 4, 11, and 19 wt% tungsten are 7.16×10^{-7} /1.03×10^{-4} A, 2.89×10^{-9} /5.96×10^{-8} A, and 1.88×10^{-10} /1.74×10^{-8} A, respectively. However, the currents of the PD with InWO having 24 wt% tungsten are outside the determination limit of the semiconductor parameter analyzer. Despite this limitation, the dark current still shows a decreasing trend. Moreover, the maximum photocurrent appears at the wavelength of 280 nm, which strongly agrees with the result of the previous bandgap analysis. The PD with InWO having 4 wt% tungsten has the highest photo/dark current ratio of 1.53×10^2. Notably, the decrease in photocurrent is more apparent.

The result can be explained by oxygen vacancies being filled by tungsten atoms; this can be confirmed from the XPS O1s result. Reducing the number of oxygen vacancies will decrease the number of electron–hole pairs (EHPs) formed by light irradiation.[20] Because the photocurrent is generated by EHPs, eliminating EHPs will decrease the photocurrent.

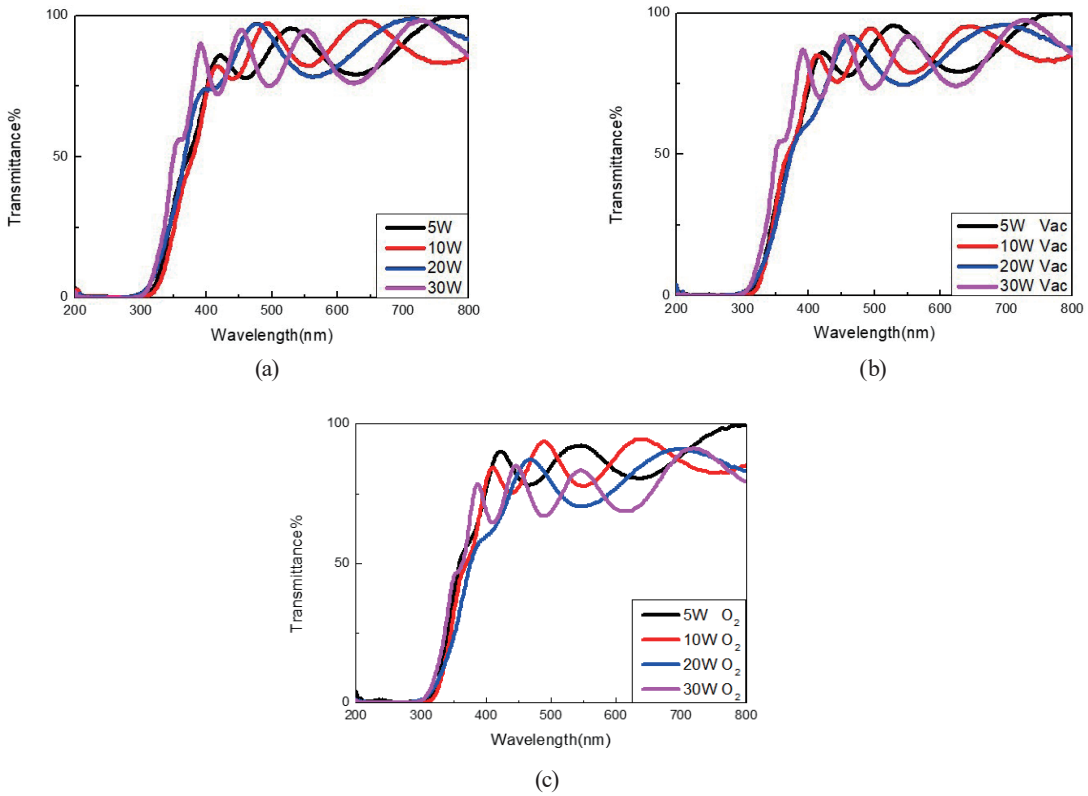

Fig. 5. (Color online) Transmittance spectra of InWO thin-film samples (a) as-deposited, (b) with vacuum thermal annealing, and (c) with thermal annealing in oxygen ambient.

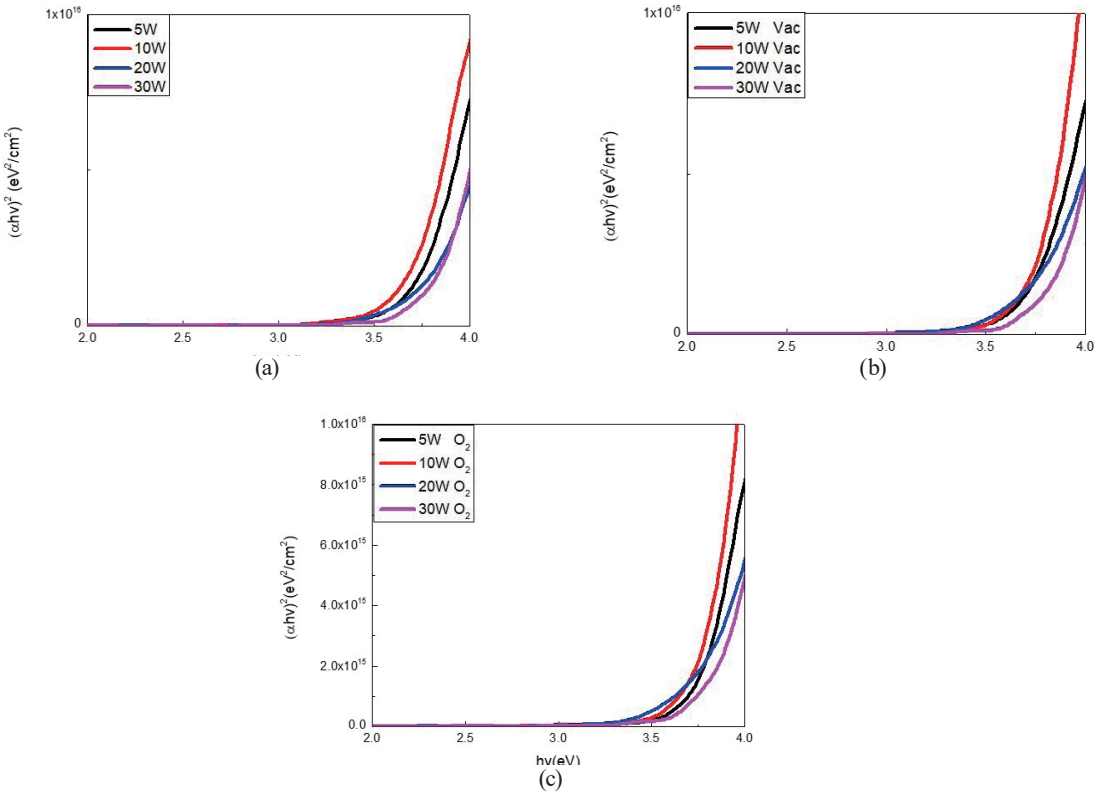

Fig. 6. (Color online) Tauc plot for InWO thin-film samples (a) as-deposited, (b) with vacuum thermal annealing, and (c) with thermal annealing in oxygen ambient.

Table 3
Calculated bandgaps (eV) of InWO thin films.

WO_3 power (W)	5	10	20	30
As-deposited	3.72	3.67	3.85	3.93
Vacuum thermal annealing	3.74	3.70	3.81	3.96
Oxygen thermal annealing	3.76	3.71	3.84	3.97

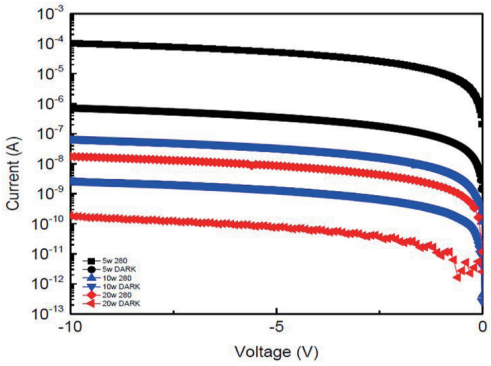

Fig. 7. (Color online) Current–voltage characteristics of unannealed InWO UV PDs with different WO_3 target cosputtering powers.

The responsivities of the InWO UV PDs with different WO_3 target cosputtering powers are illustrated in Fig. 8. On the basis of the maximum responsivity, the UV-to-visible rejection ratio was defined as the responsivity to 290 nm divided by the responsivity to 500 nm with −10 V bias applied to the top electrode. The characteristics of unannealed InWO UV PDs with different WO_3 target cosputtering powers are listed in Table 4. The PD with InWO with 4 wt% tungsten has both the highest rejection ratio and the highest responsivity. This result indicates that increasing the number of oxygen vacancies will improve the performance of the InWO UV PDs.

The time dependence of the response of InWO UV PDs with different WO_3 target cosputtering powers is shown in Fig. 9. To compare the switching speed and repeatability, all samples were tested for three cycles. Each cycle was illuminated by a xenon lamp with a wavelength of 290 nm for 50 s, and then the xenon lamp was switched off for 100 s. Table 5 shows the switching speed of each sample. The results indicate that the responsivity and switching properties of InWO UV PDs show opposite trends.

Figures 10 and 11 respectively show the current–voltage characteristics and responsivities of InWO UV PDs thermally annealed in different gas ambients. Figures 12 and 13 show the switching characteristics of InWO UV PDs thermally annealed in different gas ambients. Tables 6 and 7 show the switching speeds of samples treated in different thermal annealing gas ambients.

As is well known, thermal annealing improves the properties of TCO thin films. Thus, the photo/dark current ratio clearly increases for all thermally annealed samples regardless of a vacuum or oxygen ambient. Figure 11 shows that the slope for the InWO UV PD with the oxygen gas ambient thermal annealing process is steepest, indicating the strongest selectivity of different wavelengths. Thus, InWO UV PDs with thermal annealing in the oxygen gas ambient shows excellent ability in sensing UV light.

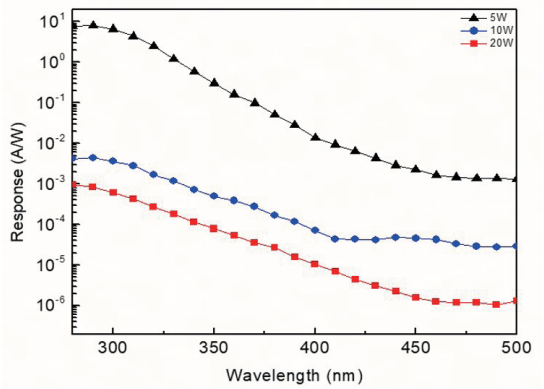

Fig. 8. (Color online) Responsivities of unannealed InWO UV PDs with different WO_3 target cosputtering powers.

Table 4
Characteristics of unannealed InWO UV PDs with different WO_3 target cosputtering powers.

Power (W)	Dark current (A)	Photocurrent (A)	Photo/dark current ratio	Responsivity (A/W)	Rejection ratio (arb. unit)
5 (4 wt%)	7.16×10^{-7}	1.03×10^{-7}	1.53×10^{2}	7.96×10^{0}	1.08×10^{3}
10 (11 wt%)	2.89×10^{-9}	5.96×10^{-8}	2.40×10^{1}	4.40×10^{-3}	4.53×10^{2}
20 (19 wt%)	1.88×10^{-10}	1.74×10^{-8}	9.25×10^{1}	9.53×10^{-4}	1.53×10^{2}
30 (24 wt%)	N/A	N/A	N/A	N/A	N/A

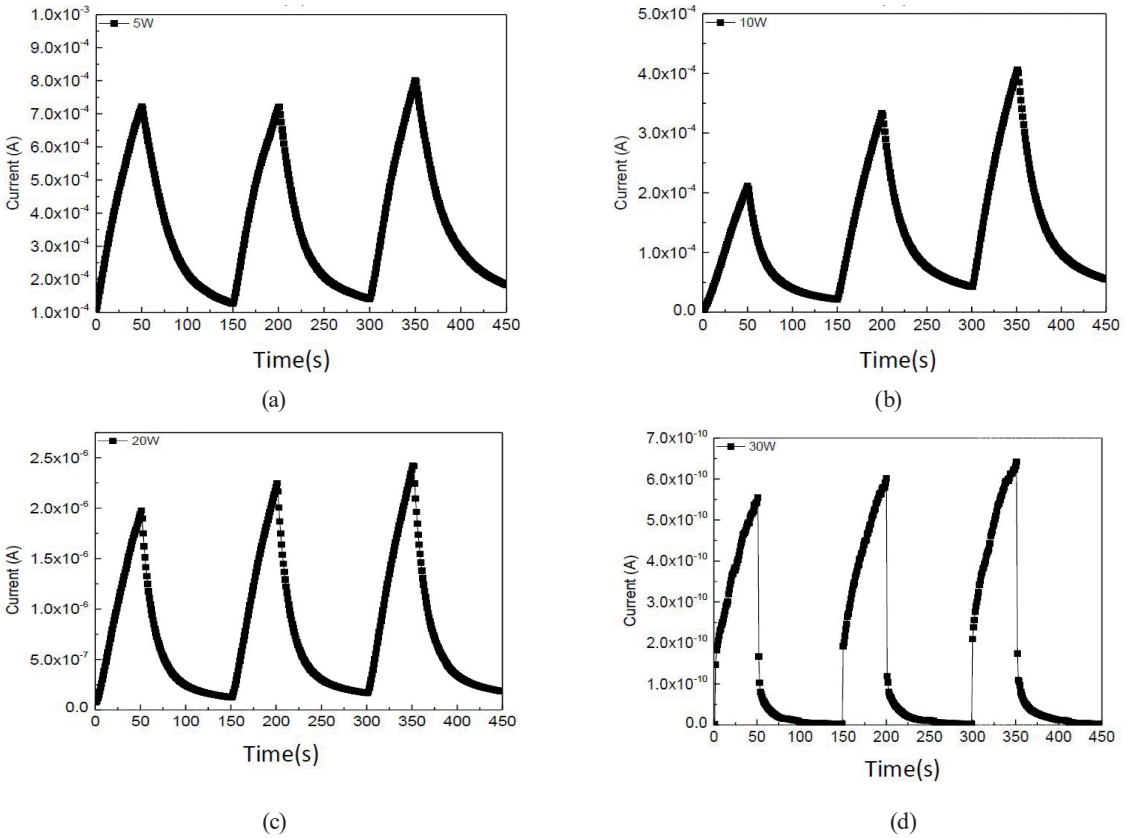

Fig. 9. Time dependence of response of unannealed InWO UV PDs with different WO_3 target cosputtering powers: (a) 5, (b) 10, (c) 20, and (d) 30 W.

Table 5
Switching speed of each unannealed InWO UV PD.

WO_3 power (W)	5	10	20	30
Rise time (s)	36	34	33	28
Fall time (s)	70	49	38	7

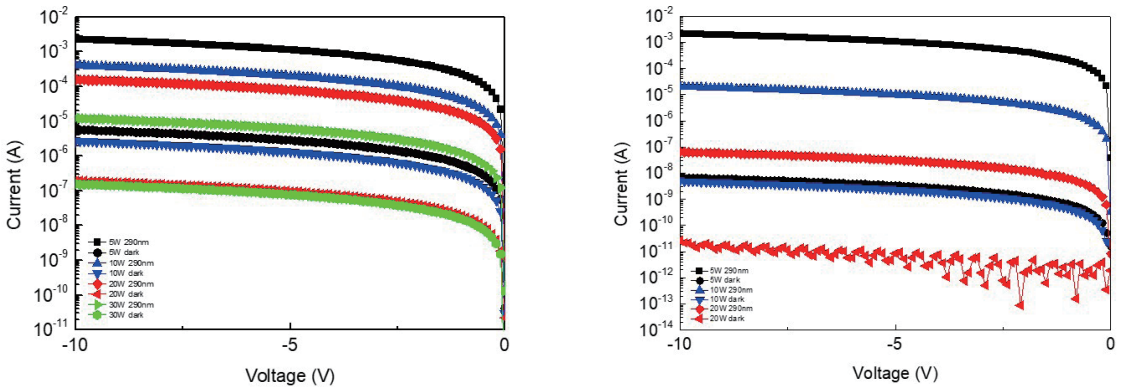

(a) (b)

Fig. 10. (Color online) Current–voltage characteristics of InWO UV PDs thermally annealed in (a) vacuum and (b) oxygen ambient.

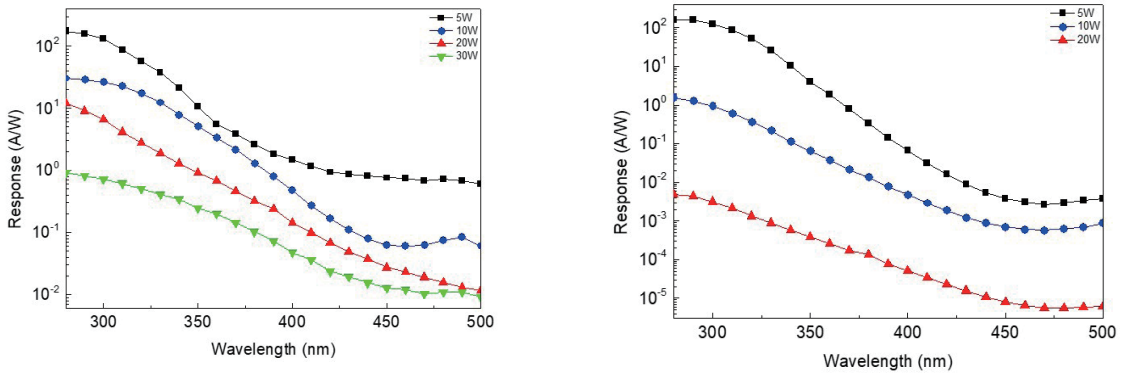

(a) (b)

Fig. 11. (Color online) Responsivities of InWO UV PDs thermally annealed in (a) vacuum and (b) oxygen ambient.

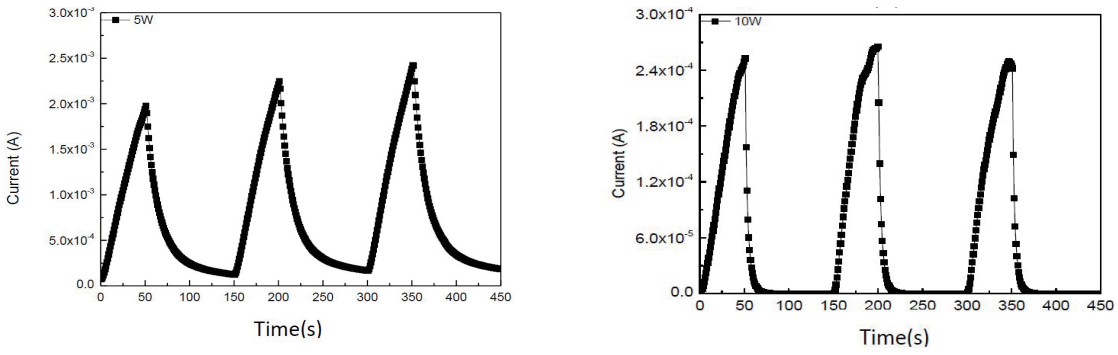

(a) (b)

Fig. 12. Time dependences of response of vacuum-annealed InWO UV PDs with WO_3 target cosputtering powers of (a) 5, (b) 10, (c) 20, and (d) 30 W.

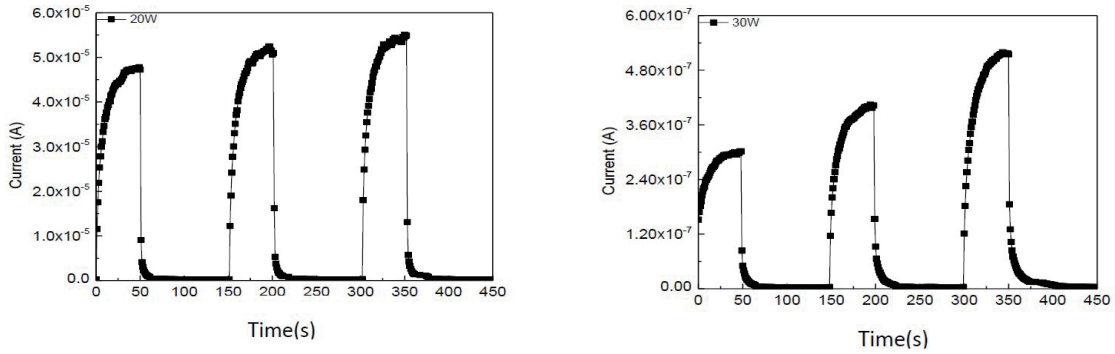

(c) (d)

Fig. 12. (Continued) Time dependences of response of vacuum-annealed InWO UV PDs with WO_3 target cosputtering powers of (a) 5, (b) 10, (c) 20, and (d) 30 W.

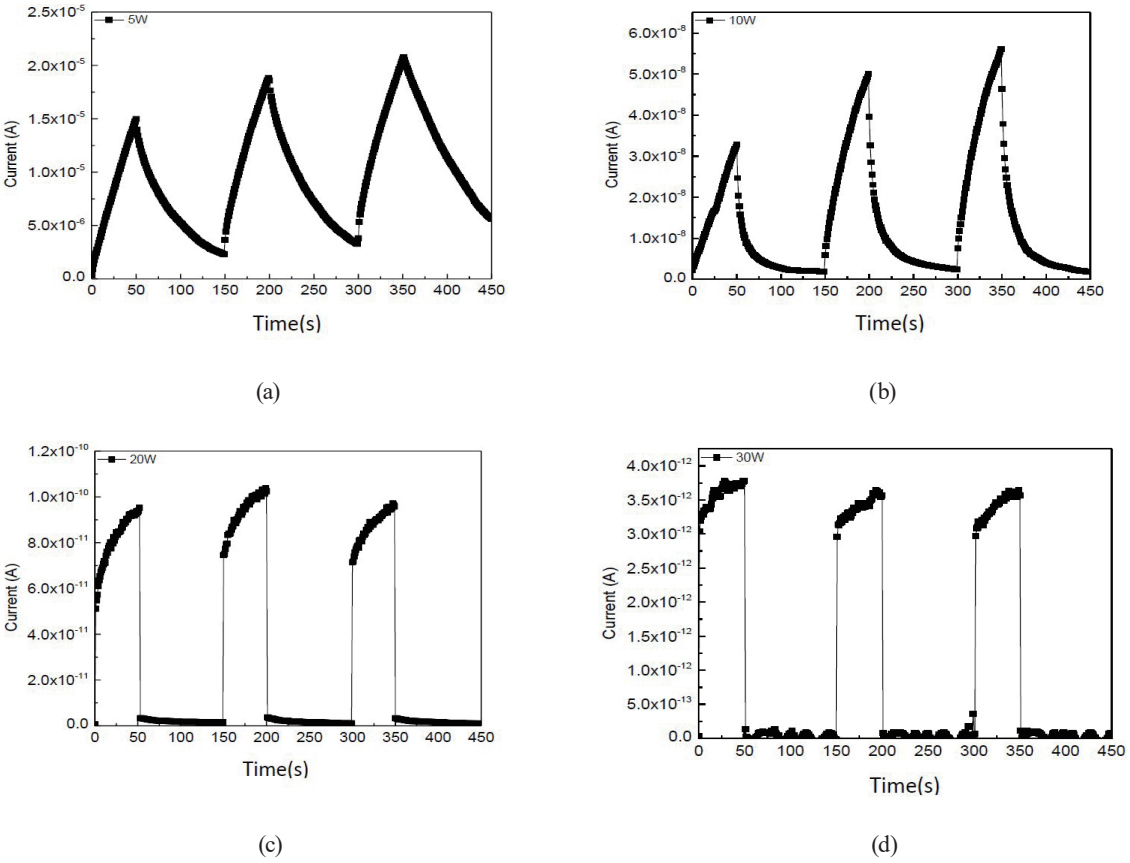

(a) (b)

(c) (d)

Fig. 13. Time dependences of response of oxygen-annealed InWO UV PDs with WO_3 target cosputtering powers of (a) 5, (b) 10, (c) 20, and (d) 30 W.

Table 6
Switching speed of InWO UV PDs thermally annealed in vacuum.

WO_3 power (W)	5	10	20	30
Rise time (s)	35	34	19	16
Fall time (s)	38	8	<1	<1

Table 7
Switching speed of InWO UV PDs thermally annealed in oxygen ambient.

WO_3 Power (W)	5	10	20	30
Rise time (s)	41	40	35	12
Fall time (s)	72	27	<1	<1

4. Conclusions

In this study, UV PDs with InWO thin films fabricated by RF magnetron cosputtering with different WO_3 target cosputtering powers were investigated. The results indicated that a lower tungsten doping ratio leads to a higher performance in terms of rejection ratio and responsivity. This was explained by the elimination of EHPs. Moreover, a higher tungsten doping ratio decreased both the dark current and the photocurrent through the suppression of oxygen vacancies by tungsten atoms.

Next, to boost the performance of InWO UV PDs, we adopted thermal annealing in a vacuum or oxygen gas ambient. The performance was improved significantly by thermal annealing in oxygen gas ambient. The results indicated that at the same annealing temperature, oxygen gas ambient greatly changed the electrical properties of InWO UV PDs. This was attributed to the extra oxygen atoms originating from the oxygen gas ambient during thermal annealing acting as the trapping centers and repairing the defect. The InWO UV PD with the In_2O_3 target sputtering power of 80 W and the WO_3 target sputtering power of 5 W and thermal annealing for 1 h in oxygen ambient has the highest performance with an ON/OFF current ratio greater than five orders of magnitude, a responsivity of 160 A/W, and a UV-to-visible rejection ratio of 4.71 × 104. Also, time-dependent switching properties were demonstrated.

Acknowledgments

The authors would like to thank the National Science and Technology Council, Taiwan, for financially supporting this research under Contract Nos. NSTC 112-2221-E-006-117-MY3 and 112-2218-E-006-010-MBK. The authors gratefully acknowledge the use of JEOL JEM-2100F CS STEM equipment belonging to the Instrument Center of National Cheng Kung University.

References

1 S.-J. Young, Y.-H. Liu, Y.-L. Chu, and J.-Z. Huang: IEEE Sens. J. **23** (2023) 12503. https://doi.org/10.1109/JSEN.2023.3272778
2 Y.-L. Chu, S.-J. Young, T.-T. Chu, A. Khosla, K.-Y. Chiang, and L.-W. Ji: ECS J. Solid State Sci. Technol. **10** (2021) 127001. https://doi.org/10.1149/2162-8777/ac3e43
3 Y.-L. Chu, S.-J. Young, D.-Y. Cai, and T-T Chu: IEEE J. Electron Devices Soc. **9** (2021) 2515. https://doi.org/10.1109/JEDS.2021.3118059
4 Y.-L. Chu, S.-J. Young, H.-R. Dai, Y.-M. Lee, A. Khosla, T.-T. Chu, and L.-W. Ji: ECS J. Solid State Sci. Technol. **10** (2021) 067001. https://doi.org/10.1149/2162-8777/ac04fc
5 Y.-L. Chu, S.-J. Young, R.-J. Ding, T.-T. Chu, T.-S. Lu, and L.-W. Ji: ECS J. Solid State Sci. Technol. **10** (2021) 037003. https://doi.org/10.1149/2162-8777/abeb53
6 Y. Zou, Y. Zhang , Y.-M. Hu, and H.-H. Gu: Sensors **18** (2018) 2072. https://doi.org/10.3390/s18072072
7 M. Liao, L. Sang, T. Teraji, M. Imura, J. Alvarez, and Y. Koide: Jpn. J. Appl. Phys. **51** (2012) 090115. https://doi.org/10.1143/JJAP.51.090115

8 D. Lin, S. Pi, J. Yang, N. Tiwari, J. Ren, Q. Zhang, P. Liu, and H.-P. Shieh: Semicond. Sci. Technol. **33** (2018) 1361. http://doi.org/10.1088/1361-6641/aabd11
9 K. Nomura, T. Kamiya, H. Ohta, T. Uruga, M. Hirano, and H. Hosono: Phys. Rev. B **75** (2007) 035212. http://doi.org/10.1103/PhysRevB.75.035212
10 T. Kamiya, K. Nomura, and H. Hosono: J. Display Technol. **5** (2009) 273 http://doi.org/10.1109/JDT.2009.2021582
11 P.-T. Liua, C.-H. Chang, and C.-J. Chang: Appl. Phys. **108** (2016) 261603. http://doi.org/10.1063/1.4954978
12 J. Pan, W. Wang, D. Wu, Q. Fu, and D. Ma: J. Mater. Sci. **30** (2014) 644. http://doi.org/10.1016/j.jmst.2013.10.023
13 R. K. Gupta, K. Ghosh, R. Patel, and P. K. Kahol: Appl. Surf. Sci. **255** (2008) 3046. http://doi.org/10.1016/j.apsusc.2008.08.077
14 G. Oh, J. Jeon, and E.-K. Kim: J. Nanosci. Nanotechnol. **16** (2016) 5109. http://doi.org/10.1166/jnn.2016.12189
15 K. F. Brennan, J. Haralson II, J. W. Parks Jr, and A. Salem: Microelectron. Reliab. **39** (1999) 1873. http://doi.org/10.1016/S0026-2714(99)00197-3
16 D.-B. Ruan, P.-T. Liu, Y.-C. Chiu, P.-Y. Kuo, M.-C. Yu, K.-J. Gan, T.-C. Chien, and S. M. Sze: RSC Adv. **8** (2018) 6925. http://doi.org/10.1039/c7ra13193c
17 Y.-R. Luo: Comprehensive Handbook of Chemical Bond Energies (CRC Press, Boca Raton, 2007) 1st ed., p. 713. https://doi.org/10.1201/9781420007282
18 H. Guo, A. Chen, W. Mi, Y. Zhang, and X. Shi: J. Mater. Chem. A. **2** (2014) 20650. http://doi.org/10.1039/c4ta05239k
19 B. D. Viezbicke, S. Patel, B. E. Davis, and D. P. Birnie III: Phys. Status Solidi B **252** (2015) 1700. http://doi.org/10.1002/pssb.201552007
20 Y. Lv, Y. Liu, Y. Zhua, and Y. Zhu: J. Mater. Chem. A. **2** (2014) 1174. http://doi.org/10.1039/c3ta13841k

About the Authors

Artde Donald Kin-Tak Lam received his B.S. degree in mechanical engineering from National Cheng Kung University (Tainan, Taiwan) in 1987 and his Ph.D. degree in electromechanical and mechanical engineering from National Sun Yat-Sen University (Kaohsiung, Taiwan) in 1993. He is a full professor in the School of Design & Straits College of Engineering of Fujian University of Technology, China, and a key talent in Fujian Province, China. His research areas include MEMS, man–machine interfaces, and sensors.

Sheng-Po Chang received his B.S. degree in electronic engineering from Southern Taiwan University of Science and Technology, Tainan, Taiwan, in 2004 and his M.S. degree in nanotechnology and microsystems engineering and Ph.D. degree in microelectronics, both from National Cheng Kung University (NCKU), Tainan, in 2006 and 2009, respectively. He is currently an assistant professor with the Department of Microelectronics Engineering, National Kaohsiung University of Science and Technology. His current research interests include II–VI and III–V optoelectronic devices, semiconductor physics, solar cells, and nanotechnology.

Chieh-Yu Kuan received his B.S. degree from National Cheng Kung University, Taiwan (R.O.C.). He is now studying for his direct Ph.D. degree from the Institute of Microelectronics at the same university. His research interests are in 2D material electronics components and applications.

Shoou-Jinn Chang received his B.S. degree from National Cheng Kung University (NCKU), Tainan, Taiwan, in 1983, his M.S. degree from the State University of New York, Stony Brook, NY, USA, in 1985, and his Ph.D. degree from the University of California, Los Angeles, CA, USA, in 1989, all in electrical engineering. From 1989 to 1992, he was a research scientist with Nippon Telegraph and Telephone Basic Research Laboratories, Musashino, Tokyo, Japan. He joined the Department of Electrical Engineering, NCKU, in 1992 as an associate professor, where he was promoted to a full professor in 1998. He served as the director of the Institute of Microelectronics, NCKU, from August 2008 to July 2011, and the deputy director of the Center for Micro/Nano Science and Technology, NCKU, from February 2006 to January 2011. He is currently the deputy director of the Advanced Optoelectronic Technology Center, NCKU. From January to March 1999, he was a Royal Society Visiting Scholar with the University of Wales, Swansea, U.K.; from July 1999 to February 2000, he was a Visiting Scholar with the Research Center for Advanced Science and Technology, University of Tokyo, Tokyo, Japan; from August to September 2001, he was a Visiting Scholar with the Institute of Microstructural Science, National Research Council, Canada; from August to September 2002, he was a Visiting Scholar with the Institute of Physics, Stuttgart University, Stuttgart, Germany; and from July to September 2005, he was a Visiting Scholar with the Faculty of Engineering, Waseda University, Tokyo. He is also an honorary professor with the Changchun University of Science and Technology, China. His current research interests include semiconductor physics, optoelectronic devices, and nanotechnology. Dr. Chang received the Outstanding Research Award from the National Science Council, Taiwan, in 2004. He is a Fellow of the Optical Society of America (OSA), the International Society for Optical Engineers (SPIE) and the Institute of Electrical and Electronics Engineers (IEEE).